JOURNAL OF CATALYSIS 149, 292–299 (1994)

Oscillating Catalytic CO Oxidation on a Platinum Field Emitter Tip: Determination of a Reactive Phase Diagram by Field Electron Microscopy

Y.-S. Lim, M. Berdau, M. Naschitzki, M. Ehsasi,[1] and J. H. Block

Fritz-Haber-Institut der Max-Planck-Gesellschaft, Faradayweg 4-6, D-14195 Berlin, Germany

Received January 3, 1994; revised June 1, 1994

A [111]-oriented Pt field emitter tip is used to study bistability and oscillations of CO oxidation by field electron microscopy (FEM) under low-pressure conditions (p_{O_2} = 4 × 10^{-4} Torr, p_{CO} = 8 × 10^{-8} to 4 × 10^{-5} Torr) in the temperature range 240 to 450 K. A *kinetic phase diagram* can be established, obtained on an FEM level with ≈2 nm lateral resolution. Below $T \approx 300$ K a region of bistability prevails, and above $T \approx 300$ K an oscillatory regime is obtained, thus yielding a cross-shaped phase diagram. These phenomena are surface plane specific and visible at the {011} planes of Pt and their surroundings. © 1994 Academic Press, Inc.

INTRODUCTION

One of the most fascinating phenomena associated with reaction systems in both homogeneous and heterogeneous phase reactions is the occurrence of temporal oscillations under conditions far from thermodynamic equilibrium. The catalytic CO oxidation on Pt-group metals is one of these heterogeneous gas reactions (1). In well-defined regions of the parameter space, defined by the external control parameters (partial pressures p_{CO} and p_{O_2}, their flow rates and sample temperature), steady states or self-sustained long-lasting isothermal oscillations of the reaction rate can be obtained.

The information about a system's steady state or oscillatory behavior can be compiled in a kind of *kinetic phase diagram*. This term has been proposed, in analogy to equilibrium thermodynamics, by Schlögl (2, 3). The concept is based on the fact that in both equilibrium and nonequilibrium phase transitions cooperative phenomena play a decisive role leading, for example, to ordered structures in the equilibrium case and to self-organizing dissipative structures in the nonequilibrium case. The occurrence of competing reactive "phases" is intimately correlated with such phenomena as instabilities, multistabilities, bifurcations, and kinetic oscillations. In the following, therefore, we denote any plot relating the system's reactivity behavior to external control parameters (p, T, . . .) as a (*reactive*) *phase diagram*. For reactions in homogeneous phase, experimental phase diagrams showing different steady states and oscillatory regimes have laid a basis for deriving mechanisms for oscillations or finding new oscillatory systems (4).

Oscillation phenomena have been investigated before at different single-crystal planes of platinum. Kinetic oscillations on the single-crystal planes of Pt(100), Pt(110), and Pt(210) are encountered in widely different regions of the parameter space (1, 5–9). The Pt(111) surface does not show oscillations for low reaction gas pressures (1, 10, 11).

Self-organizing oscillations may develop if a proper feedback reaction is added to a system that exhibits bistability. For CO oxidation bistability appears due to the Langmuir–Hinshelwood reaction steps (4, 12–14). Various feedback reactions are presently under discussion for those single-crystal surfaces that reveal reactivity oscillations during CO oxidation. The feedback reaction for Pt(100) and Pt(110) (1, 5, 6, 15) is deemed to be the reversible reconstruction of the surface, whereas for Pt(210) a more complicated process involving faceting is proposed (16). For Pd(110) all investigations agree that the feedback reaction is the reversible formation of subsurface oxygen (17). Common to all these feedback reactions is their direct modulation of the oxygen sticking probability. Other work also on Pt(100) (18), Pt(110) (19), and Pt(210) (20) indicates the existence of subsurface oxygen. Due to these findings the reversible formation of subsurface oxygen may be responsible for oscillations on large single-crystal surfaces.

The use of a field emitter tip as a catalyst permits a direct comparison of different single-crystal planes in one experiment. At such an emitter many different planes from low to high index symmetries are exposed to the reacting gas simultaneously.

[1] Present address: Institut für Physikalische und Theoretische Chemie der Freien Universität Berlin, Takustrasse 3, D-14195 Berlin.

0021-9517/94 $6.00

Another advantage of the field emitter tip is that the small single-crystal planes model a technical catalyst better than a large single-crystal surface. The surface of these "real" catalysts consists of surface structures of many different orientations. Contrary to experiments with large single-crystal surfaces processes on the field emitter tip as well as on "real" catalysts may be influenced by the edges of the microscopic grains. Furthermore, for a comparison it is important to know the minimum surface size required to yield the same properties as an infinitely large surface.

The present contribution uses field electron microscopy (FEM) *in situ* to investigate the phenomenon of bistability between two steady states causing hysteresis and self-sustained oscillations during CO oxidation on the ensemble of small single-crystal surface areas exposed at a Pt field emitter tip.

EXPERIMENTAL

The experimental technique and the procedures used to evaluate catalytic surface reactions *in situ* by FEM have been described in detail elsewhere (21). The present experiments were performed in an ultrahigh vacuum (UHV) chamber used as a flow reactor with a base pressure of 1×10^{-10} Torr. The catalyst was a platinum tip prepared by electrochemical etching in 10% KCN solution. After this process the sample was cleaned by field evaporation in a Ne–H_2 mixture ($p_{Ne} = 5 \times 10^{-5}$ Torr, $p_{H_2} = 5 \times 10^{-7}$ Torr), subsequent heating in an UHV to red glow, and repeated field evaporation. This procedure gives a clean tip with well-defined crystallographic orientations. The diameter of our [111]-oriented Pt field emitter tip was approximately 350 nm.

CO and oxygen were admitted to the reaction chamber by an electronically regulated gas inlet system. Prior to admission to the chamber, these high-purity gases (CO 99.997%, O_2 99.999%) were further purified by several molecular sieve traps and a final liquid nitrogen cold trap. The purity of the gases was monitored by means of a quadrupole mass spectrometer. The pressure of the reactants was determined with a spinning-rotor gauge and an ion gauge. The temperature of the emitter was measured and regulated by electronically monitoring the resistance of the heating loop and was controlled in the range 80 to 1000 K to within an accuracy of ±1 K. Field strength values were evaluated by determining the best image voltage for Ne at 80 K, which corresponds to 35 V/nm (22).

The electron current in the field electron microscope was amplified by a channel plate and made visible on a luminescent screen. The field emission images were monitored by a CCD camera and recorded on videotape. Concurrently the total emission current detected on the channel plate was converted to a frequency signal by a voltage-to-frequency converter and recorded on the audio track of the videotape. Thus, the overall dynamics of the reaction could be determined with a temporal resolution of 40 ms, i.e., 25 video frames per second.

RESULTS

In the field electron microscope, the local electron work function Φ_{hkl} determines the field emission current I. A high local field emission current results in a bright image area. Smooth surfaces have a high work function and thus yield a low field emission current. For platinum the work function Φ of the single-crystal surfaces (23) is 5.95 eV for Pt(111), 5.85 eV for Pt(100), and 5.70 eV for Pt(110). Surfaces with higher index planes, like Pt(210), have an even lower work function.

The *oxygen-covered* platinum surface shows a relatively *large increase* in the work function [up to 700 meV (24–27)], whereas the increase due to the *CO-covered* surface is *smaller* [up to 300 meV (24, 25, 28–30)]. Work function changes due to adsorption are face specific and, in most cases, not linearly dependent on surface coverages. This makes a quantitative correlation between the measured field emission current I and the actual surface coverage difficult. For all cases, however, the increase in Φ is higher for adsorbed oxygen than for adsorbed CO. Aside from Pt(111), the clean platinum surface has a much lower work function than a covered one (24–26, 28–31). A change in brightness of a particular surface in the field electron microscope from dark to light correlates with a transition from high oxygen coverage to high CO coverage. The uncovered surfaces appear very bright. One can thus employ the distinct changes in the work function during the adsorption of CO and oxygen at the various single-crystal planes of the emitter to obtain qualitative information about the adsorbates.

From former experiments with large single-crystal planes it is known (1) that the oxygen-covered platinum surface has a high catalytic reactivity, while the CO-covered surface poisons the reaction by preventing dissociative oxygen chemisorption. It has previously been shown that on single-crystal surfaces the work function change $\Delta\Phi$ follows the reaction rate in all details (32, 35). We take advantage of this intimate correlation for the present work in FEM at a field emitter tip to directly monitor the selectivity of the surface to kinetic rate oscillations with a very high lateral resolution [approximately 2 nm (32–34)].

Figure 1 gives an example of hysteresis and oscillations in the reaction rate as indicated by the experimental field electron current I. The total emission current is obtained at constant oxygen pressure and temperature during variation of the CO pressure. For low CO pressures the surfaces of the tip are covered predominantly by oxygen (oxygen-side); for higher CO pressures, the surface is

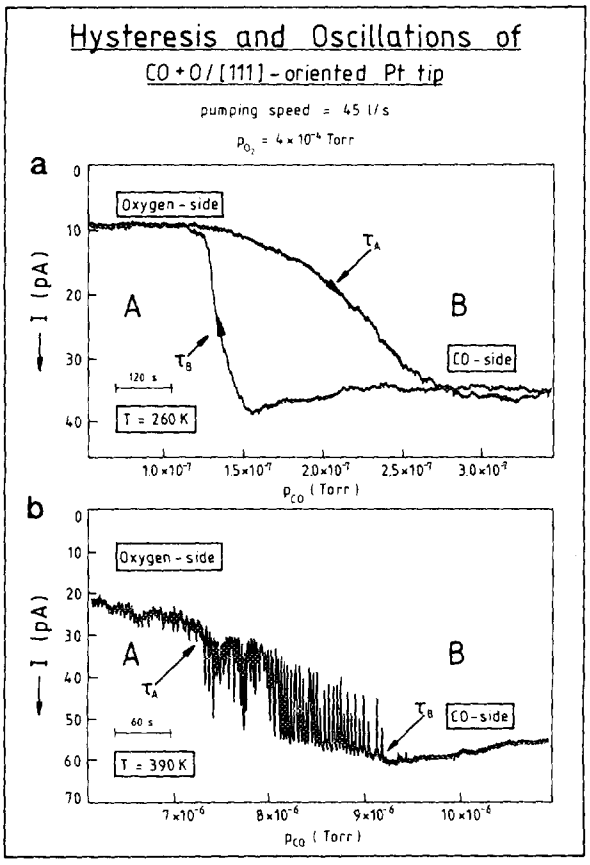

FIG. 1. (a) Hysteresis of the total field electron current from the emitter surface with $\tau_A > \tau_B$ at a constant oxygen pressure of 4×10^{-4} Torr below 300 K during variation of the CO pressure. (b) Oscillatory behavior with $\tau_A < \tau_B$ at an oxygen pressure of 4×10^{-4} Torr above 300 K for increasing CO pressure. (A) Monostable region of high catalytic reactivity, (B) monostable region of low catalytic reactivity. The different reactive states of the Pt tip for the CO-side and oxygen-side and an oscillatory cycle are displayed in FEM images in Fig. 2.

poisoned by CO (CO-side). At temperatures below 300 K the measurements show hysteresis; above 300 K, oscillatory behavior is observed. The hysteresis and oscillations shown in Fig. 1 are similar to the results of experiments on a large Pd(110) single crystal (35).

The points τ_A and τ_B depicted in Fig. 1 are defined and explained below. In general, τ is a point of transition (or bifurcation) between two qualitatively different states of the system: while an external control parameter is changing, the system originating in the monostable region A or B loses its stability at the transition point. The subscript thus denotes the monostable region in which the system is found before starting the scan.

For hysteresis (Fig. 1a), the points τ_A and τ_B have the following meaning. For constant p_{O_2} and T the value τ_A describes the CO pressure at which, with increasing p_{CO}, the stable steady state of high catalytic reactivity reaches a point of marginal stability. For $p_{CO} \geq \tau_A$ the reaction approaches the steady state of low reactivity, which is monostable for this CO pressure (monostable region B). Likewise this steady state becomes unstable with *decreasing* p_{CO} at point τ_B. A further decrease in p_{CO} reinstalls, at $p_{CO} \leq \tau_B$, the stable steady state of high reactivity (monostable region A). For hysteresis three regions of stability thus exist: the monostable region A, the monostable region B, and a region of bistability for CO pressures between τ_A and τ_B.

In the case of *oscillations* (Fig. 1b), τ_A and τ_B represent the limits of the oscillatory region.

Experimentally the value of τ_B can be located quite precisely since the transition occurs in a narrow pressure range. There is more leeway in fixing the location of τ_A as this is a more gradual transition (Fig. 1a). For the logarithmic CO pressure scale in the phase diagram (see Fig. 4), however, the precise position of τ_A is of minor importance. For the hysteresis in Fig. 1a (and Fig. 3) the inflection points of the I-vs-p_{CO} curves have been chosen as the positions of τ_A and τ_B. Even if the transition points were obtained in a different way from the curves and thus shifted on the pressure scale, the qualitative shape of the constructed phase diagram (see Fig. 4) would remain nearly the same.

An increasing effect is encountered regarding the onset of oscillations during the reverse scan of the CO pressure (not shown in Fig. 1b). In this case oscillations are obtained only if the CO pressure is decreased immediately after oscillations cease coming from lower CO pressures. An increase in p_{CO} far beyond τ_B prevents oscillations from occurring during the reverse scan. We interpret this effect in light of the reactivity of the various surface planes with different $\{hkl\}$. For CO pressures close to τ_B some surface planes may still be active or covered with oxygen, hence triggering oscillations during the reverse scan, whereas at higher p_{CO} a completely CO-covered surface would prevent the dissociative oxygen adsorption at $p_{CO} \leq \tau_B$.

Figure 2 displays FEM images obtained at 390 K which correlate with the measurements in Fig. 1b. The crystallographic orientation of the {001} and {011} planes of a [111]-oriented Pt tip are sketched in Fig. 2.1a. The smaller high-index surfaces are indicated by unfilled ovals. The {011} planes [encompassing the (110), (101) and (011) planes of the field emitter tip], together with the surrounding high-index planes, have a low work function in comparison to the (111) and {001} surfaces. In the present experimental setting these areas thus appear bright, even for a nearly fully oxygen-covered surface (Fig. 2.1b). For higher CO pressures (Fig. 2.1c) the tip is covered predominately by CO, resulting in a larger bright area around the {011} surfaces. In both cases (Figs. 2.1b and 2.1c) the central (111) plane appears dark because the field strength in this

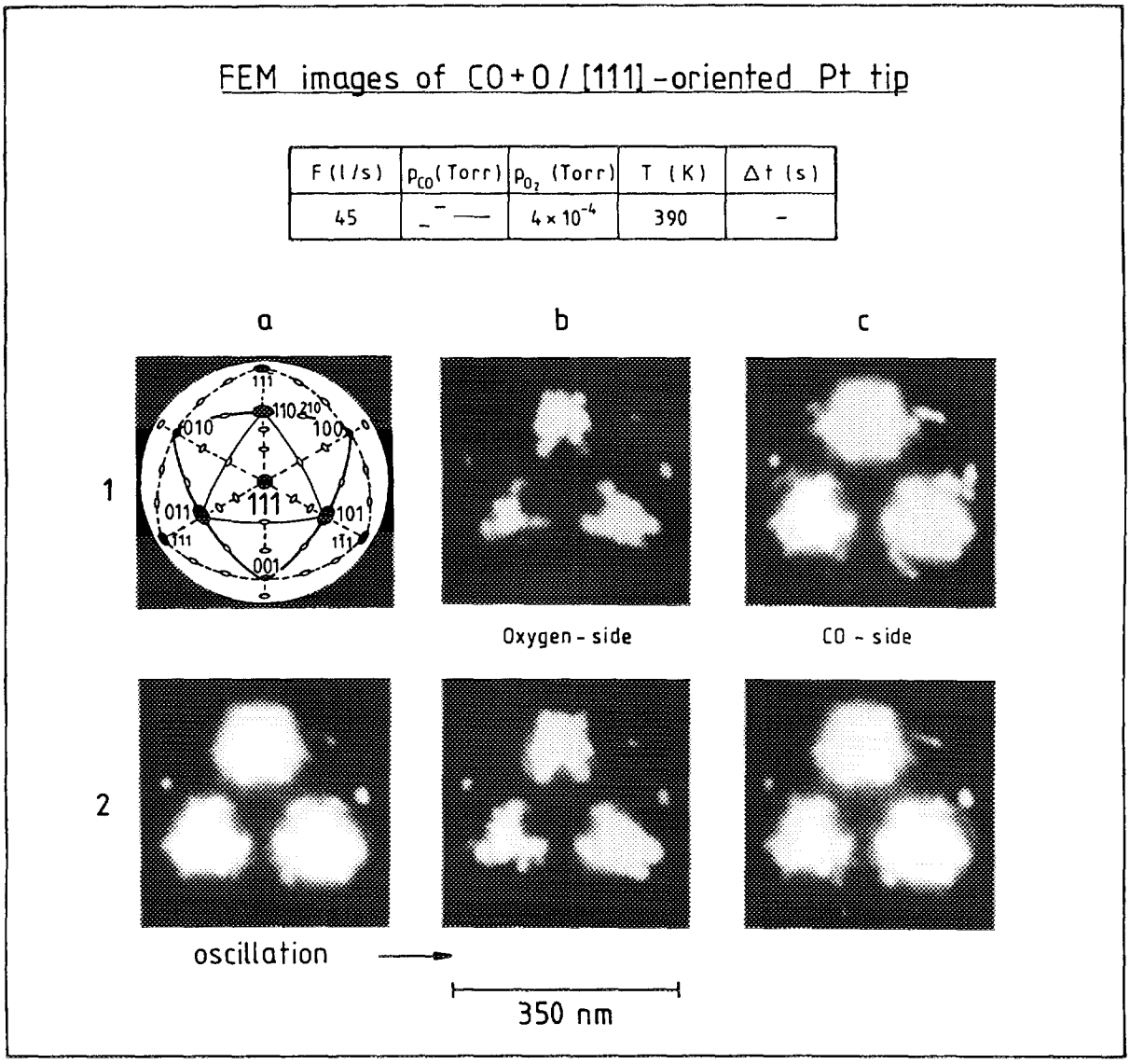

FIG. 2. FEM images of the Pt tip taken during the ongoing catalytic surface reactions. The field strength at the tip is approximately 4 V/nm. The CO pressures for the respective images are (1b) 4.2×10^{-6} Torr, (1c) 10.7×10^{-6} Torr, and (2) 6.8×10^{-6} Torr.

area is too low for the emission of field electrons due to the local tip radius.

Figure 2.2 presents one oscillatory cycle at 390 K. Evidently the surface regions near the {011} planes and their surroundings are reactive and responsible for the oscillatory behavior. The (011) plane on the lower left is especially prominent in the change in brightness during this oscillatory cycle. The behavior on the {001} planes and their surroundings is difficult to observe on this [111]-oriented tip, because these areas are visible only at the border of the tip due to its relatively large diameter (see, for example, the upper right of each image in Fig. 2).

Figure 3 shows the results of a series of CO oxidation experiments at different sample temperatures. The CO pressure was scanned in each direction for 15 min. For temperatures below 300 K (left column of Fig. 3) only hysteresis is observed, whereas above 300 K (right column of Fig. 3) rate oscillations appear. As the temperature is increased the bistable region with $\tau_A > \tau_B$ shifts to higher p_{CO} and narrows until, at $T \approx 300$ K, τ_A equals τ_B (crossing point). With a further temperature increase τ_A and τ_B reverse sides, whereupon oscillations occur with $\tau_A < \tau_B$. The crossing of τ_A and τ_B can be seen directly in Fig. 1. For the sake of clarity τ_A and τ_B are not depicted in Fig. 3. The frequency of these oscillations increases with temperature, similar to the results of measurements

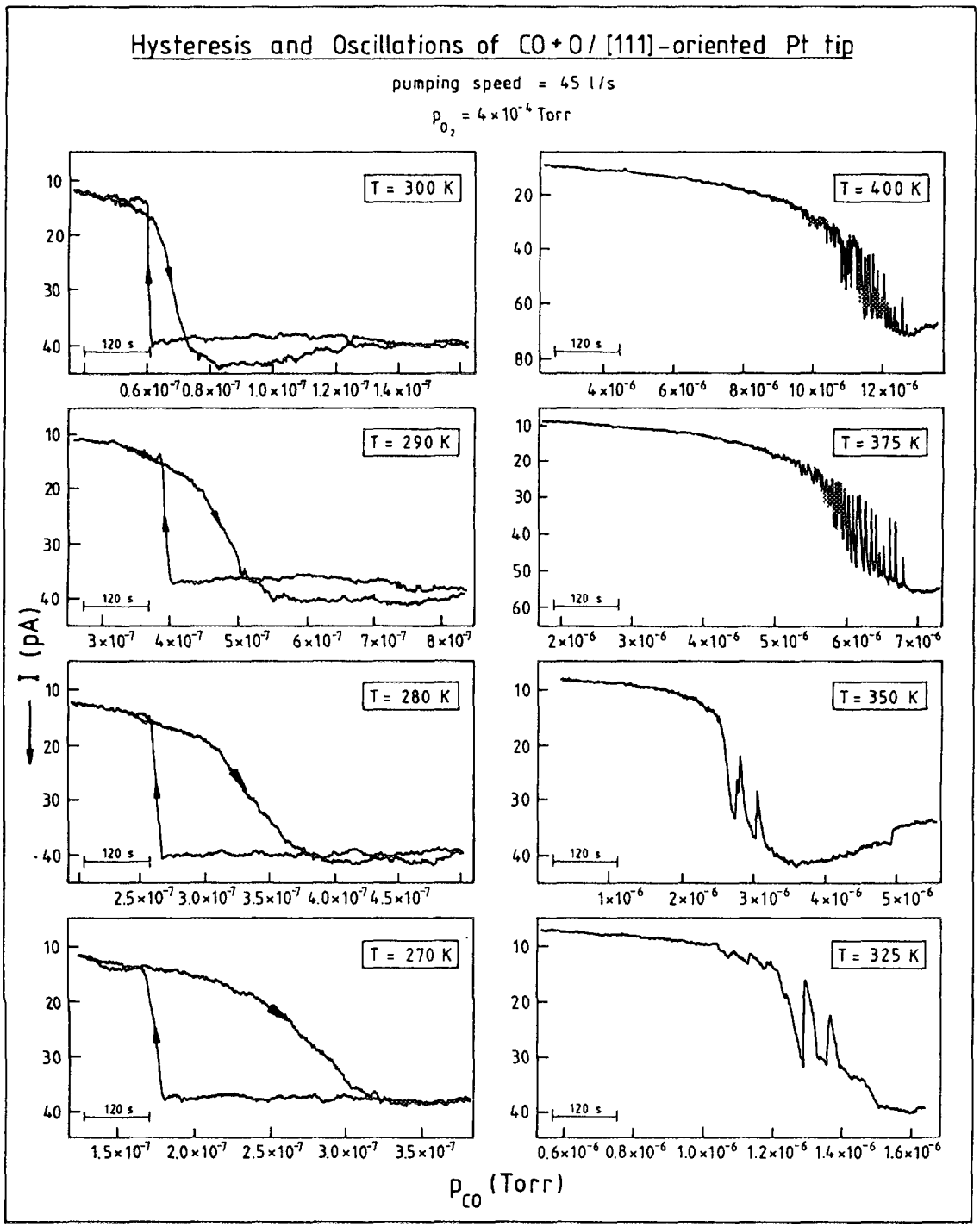

FIG. 3. Total field electron current from the emitter surface as a function of CO partial pressure during CO oxidation at different temperatures. The hysteresis loops below 300 K narrow with increasing temperature (left column); above 300 K, oscillations occur (right column, for clarity the reverse scans to lower p_{CO} are not shown).

of oscillatory systems on large single-crystal planes (32, 36–38).

In Fig. 3 it can be seen that the transition from the oxygen-side to the CO-side always occurs in a gradual, smooth manner. This behavior is also visible in the corresponding FEM images. With increasing CO pressure those regions on the {011} planes and their surroundings covered by CO increase in size. The reverse transition

back to the oxygen-covered surface takes place more abruptly. In the oscillatory region of parameter space, a front grows and shrinks over the {011} region with the {123} planes as the source. Qualitatively a different behavior can be observed above 400 K. Above this temperature the oscillations have a smaller amplitude and the fronts move back and forth a smaller distance. Observing oscillations for a CO scan above 450 K thus becomes difficult. Compared with temperatures below 400 K, the maximum value of field electron current encountered during the CO pressure scan above 400 K becomes progressively greater with increasing temperature. This is due to the concurrent increase in the number of empty surface sites. Above 400 K the tendency for a more pronounced morphological change in the surface also increases with temperature, as observed before by Gorodetskii *et al.* (39). At 500 K additional spots in the FEM images appear which may be due to the rough surface. A combined analysis of the FEM method with present field ion microscopy (FIM) studies will yield further insight into the temperature dependence of the CO oxidation.

The experimentally determined values of τ_A and τ_B are presented as a function of the reciprocal temperature in Fig. 4. On connecting the values of τ_A and those of τ_B, we obtain a cross-shaped phase diagram with four regions:

1. The monostable region A, where the reaction is in the steady state of high reactivity with high oxygen coverage
2. The monostable region B, where the reaction is in the steady state of low reactivity and predominantly poisoned by CO
3. The bistable region (lower right) with the steady state of high or low reactivity (with due consideration to the limited experimental time)
4. The oscillatory region (upper left) with periodic change of the reaction rate.

The observed cross-shaped phase diagram is discussed in detail in the following section.

DISCUSSION

With the kinetic phase diagram presented in Fig. 4 the CO oxidation dynamics on the Pt field emitter tip can be described in parameter space at a particular oxygen partial pressure. The FEM images show that the observed phenomena (hysteresis and oscillations) are located at the {011} planes and their surroundings.

In addition to the present experimental data on the *small* single-crystal planes of the tip, Fig. 4 also depicts preceding measurements of rate oscillations on a *large* Pt(110) single-crystal surface (filled circles). These data are interpolated from a series of p_{CO}-vs-$1/T$ curves at different oxygen pressures from a contribution of Eiswirth *et al.* (6, Fig. 2). In this work the oscillatory behavior is also observed with the aid of the work function change $\Delta\Phi$ using a Kelvin probe. These authors found oscillations at parameter values that are similar to those found recently in photoelectron emission microscopy (PEEM) observations of oscillations on a large Pt(110) single-crystal plane (40, 41). Since the existence regions of oscillations on the large Pt(110) single-crystal planes and field emitters agree, we hypothesize that the {011} regions are responsible for the observed behavior of the CO oxidation. Further, this comparison indicates that electrostatic field effects in FEM measurements are of minor importance.

Notwithstanding the question of the existence regions of the observed oscillations, it is certainly clear from the FEM images that the observed hysteresis and oscillations are localized at the {011} planes and their surroundings. This crystallographic specificity toward oscillations in CO oxidation has been observed before (21).

An advantage of the FEM method is the possibility of simultaneously studying the behavior of different single-crystal planes. This may be employed for gaining insight into the role of defects on large single-crystal surfaces. During CO oxidation on large single-crystal surfaces the photoelectron microscope can be used to observe spatiotemporal structures like islands, target patterns, or spirals (41, 42). In most cases small inhomogeneities are visible at the center of these structures. The exact nature of these surface defects on large single crystals is still unclear. These defects can act as a pacemaker or leading center for the observed spatiotemporal structures in oscillatory reactions. It is likely that the most active plane on the tip is also the source of the pacemaker on large single-crystal surfaces. In addition to their importance for oscillation phenomena, these planes may also be very active for catalytic reactions.

Two other aspects need to be discussed concerning hysteresis and oscillations on the tip. When comparing the field emitter with large single-crystal planes, one has to consider the fact that the different planes of the field emitter do not act independently. In studies with field emitter tips there exists the possibility that adjacent crystallographic planes of different symmetry interfere with each other due to the interplane surface diffusion of the reacting adsorbed CO and, to a certain extent, the adsorbed oxygen. Thus an oscillation on a certain plane may trigger oscillations on other ones which, if isolated, would not show oscillations under the given conditions of the external control parameters. One must therefore differentiate between autonomous oscillations and forced oscillations, which are due to the formation of traveling reaction fronts triggering the overall oscillations. Only autonomous oscillations, which we can see in the present work can be compared with the results on large single crystals.

The second aspect concerns the time dependence of the observed data. Concerning hysteresis, in general on

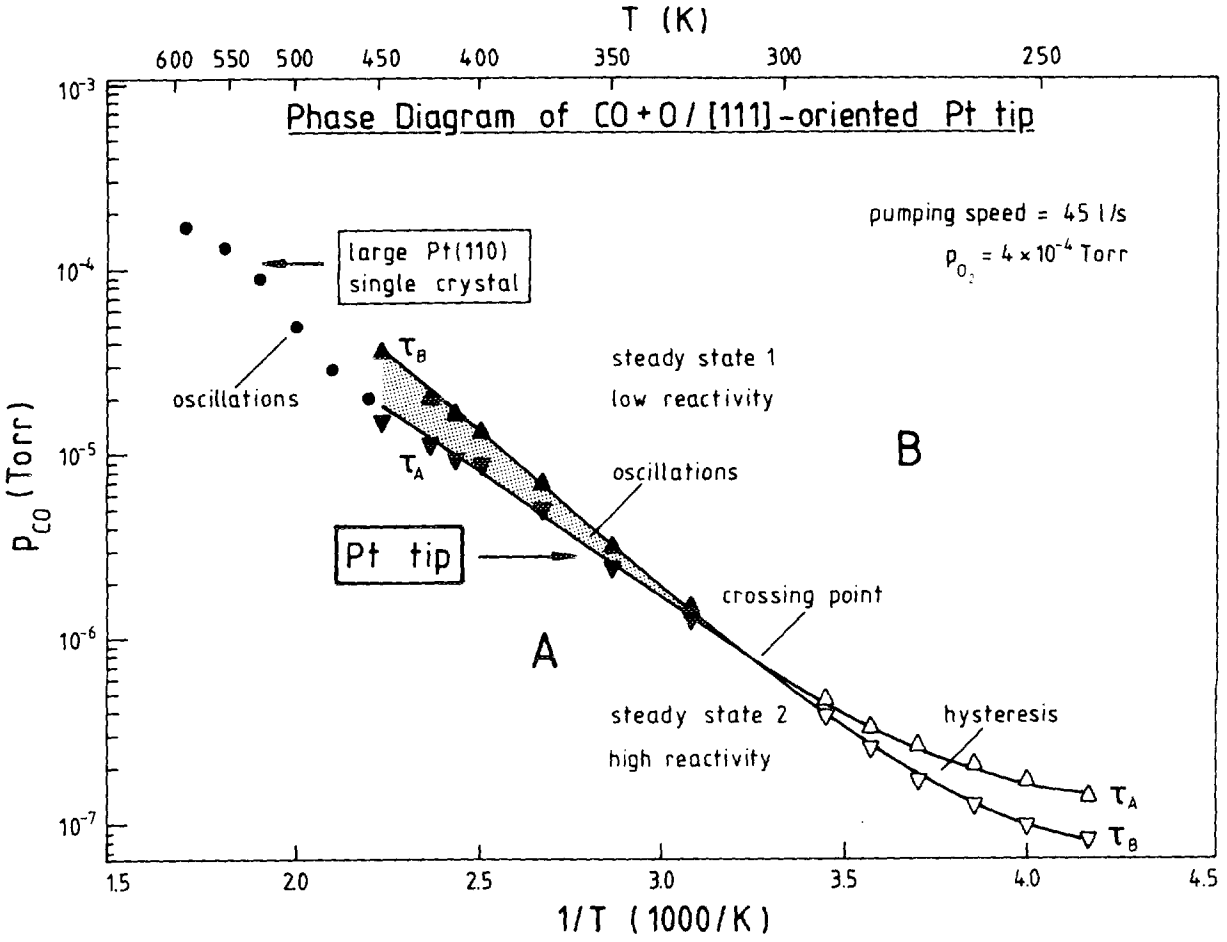

FIG. 4. Cross-shaped phase diagram of the [111]-oriented Pt tip. Hysteresis and oscillation phenomena are located around the {011} surfaces of the tip. Additional literature values (6) for the oscillation on a large Pt(110) surface are given for higher temperature. The field strength in the FEM experiment is 4 V/nm.

has to ask to what extent the width of the hysteresis loop depends on the scanning speed of the external control parameter. If the scanning speed of such a parameter (p_{CO} in our case) is decreased, the hysteresis region narrows. This has been observed in earlier investigations on single-crystal planes (35). In some cases oscillations even developed in confined regions of the hysteresis loop. For longer scanning times it is possible that the crossing point at 300 K could be shifted somewhat to lower temperatures (4).

The significance of kinetic phase diagrams for studying bistability and oscillations has been extensively discussed for CO oxidation on Pd(110) (35). Although an *isothermal* cross-shaped phase diagram was the subject of the former work, some of the general conclusions can be applied to the present phase diagram evaluated at different temperatures.

In general, the gradual transition from hysteresis to oscillation phenomena during the variation of an external control parameter manifests the operation of a feedback process (4, 12–14). Modeling the CO oxidation solely in the framework of the Lagmuir–Hinshelwood mechanism results in hysteresis (bistability). A bifurcation analysis of the corresponding steady-state equations shows clearly that bistability exists in the temperature range where adsorption of CO is permitted. The lines connecting the bifurcation points τ_A and τ_B, respectively, can cross only if an additional feedback becomes operative. At higher temperatures, this feedback process results in oscillations, their frequency increasing with temperature. Investigations of homogeneous and heterogeneous oscillatory reactions have so far not yielded a cross-shaped phase diagram dependent on temperature [cf. (4)]. In the present cross-shaped phase diagram one of the control parameters is the temperature of the catalyst. Different temperatures lead to different rates of adsorption, desorption, diffusion, and reaction of CO and oxygen on each crystallographic surface. The feedback process can therefore be quite com-

plicated. Determination of the exact nature of the feedback process will require additional experimental and theoretical investigations. It may be that also for this system one of the feedback processes that are presently under discussion (reversible formation of subsurface oxygen, reconstruction of the surface) plays an important role.

CONCLUSIONS

In the present work a small single-crystal field emitter tip with a diameter of 350 nm exhibits a reproducible appearance of the hysteresis and oscillations in parameter space. The *kinetic phase diagram* describes different reactive regions in this control parameter space. Studies of the oscillatory region for a large Pt(110) single-crystal surface compares favorably with the present work. This shows clearly that the properties of large single-crystal surfaces are also represented by the small surfaces on a field emitter tip.

The experimental results demonstrate the suitability of the field electron microscope for studies of catalytic reactions. With the help of similar investigations the most active planes for a particular reaction can be determined, providing important insight into catalytic reactions. Furthermore, such studies can be used as a link between early work with oscillatory CO oxidation on carrier catalysts (43) and that on large single-crystal planes. The high lateral resolution with FEM down to 2 nm gives detailed information about the interplay of neighboring crystallographic surfaces which can result in triggering face-specific catalytic reactions by chemical waves.

ACKNOWLEDGMENTS

Valuable discussions with V. Gorodetskii are acknowledged. We thank T. Rebitzki for the critical reading of the manuscript.

REFERENCES

1. Ertl, G., *Adv. Catal.* **37,** 213 (1990).
2. Schlögl, F., *Z. Phys.* **248,** 446 (1971); *Z. Phys.* **253,** 147 (1972).
3. Schlögl, F., *Ber. Bunsenges. Phys. Chem.* **84,** 351 (1980).
4. De Kepper, P., and Boissonade, J., *in* "Oscillations and Traveling Waves in Chemical Systems," (R. J. Field and M. Burger, Eds.), Chap 7. Wiley, New York, 1985.
5. Ertl, G., Norton, P. R., and Rüstig, J., *Phys. Rev. Lett.* **49,** 177 (1982).
6. Eiswirth, M., Möller, P., Wetzel, K., Imbihl, R., and Ertl, G., *J. Chem. Phys.* **90,** 510 (1989); Ladas, S., Imbihl, R., and Ertl, G., *Surf. Sci.* **197,** 153 (1988).
7. Ehsasi, M., Rezaie-Serej, S., Block, J. H., and Christmann, K., *J. Chem. Phys.* **92,** 7596 (1990).
8. Ehsasi, M., Seidel, C., Ruppender, H., Drachsel, W., Block, J. H., and Christmann, K., *Surf. Sci.* **210,** L198 (1989).
9. Imbihl, R., Cox, M. P., and Ertl, G., *J. Chem. Phys.* **84,** 3519 (1986).
10. Yeates, R. C., Turner, J. E., Gellman, A. J., and Somorjai, G. A., *Surf. Sci.* **149,** 175 (1985).
11. Ehsasi, M., Matloch, M., Frank, O., Block, J. H., Christmann, K., Rys, F. S., and Hirschwald, W., *J. Chem. Phys.* **91,** 4949 (1989).
12. Epstein, I. R., and Luo, Y., *J. Chem. Phys.* **95,** 244 (1991).
13. Boissonade, J., and de Kepper, P., *J. Phys. Chem.* **84,** 501 (1980).
14. Orbán, M., Dateo, Ch., de Kepper, P., and Epstein, I. R., *J. Am. Chem. Soc.* **104,** 5911 (1982).
15. Krischer, K., Eiswirth, M., and Ertl, G., *Surf. Sci.* **251/252,** 900 (1991).
16. Sander, M., Imbihl, R., and Ertl, G., *J. Chem. Phys.* **95,** 6162 (1991).
17. Ladas, S., Imbihl, R., and Ertl, G., *Surf. Sci.* **219,** 88 (1989).
18. Rotermund, H. H., Lauterbach, J., and Haas, G., *Appl. Phys. A* **57,** 507 (1993).
19. Vishnevskii, A. L., and Savchenko, V. I., *React. Kinet. Catal. Lett.* **38,** 167 (1989).
20. Moldenhauer, S., *et al.*, in press.
21. Gorodetskii, V., Block, J. H., Drachsel, W., and Ehsasi, M., *Appl. Surf. Sci.* **67,** 198 (1993).
22. Müller, E. W., and Tsong, T. T., "Field Ion Microscopy, Principles and Applications," p. 12. Elsevier, New York, 1969.
23. Rotermund, H. H., Jakubith, S., Kubala, S., von Oertzen, A., and Ertl, G,. *J. Electron Spectrosc. Relat. Phenom.* **52,** 811 (1990).
24. Ehsasi, M., Ph.D. thesis, FU Berlin (1989).
25. Imbihl, R., Ladas, S., and Ertl, G., *Surf. Sci.* **206,** L903 (1988).
26. Derry, G. N., and Ross, P. N., *J. Chem. Phys.* **82,** 2772 (1985).
27. Griffiths, K., Jackman, T. E., Davies J. A., and Norton, P. R., *Surf. Sci.* **138,** 113 (1984).
28. Norton, P. R., Goodale, J. W., and Selkirk, E. B., *Surf. Sci.* **83,** 189 (1979).
29. Behm, R. J., Thiel, P. A., Norton, P. R., and Ertl, G., *J. Chem. Phys.* **78,** 7437 (1983).
30. Thiel, P. A., Behm, R. J., Norton, P. R., and Ertl, G., *J. Chem. Phys.* **78,** 7448 (1983).
31. Gorodetskii, V. V., and Savchenko, V. I., *Dokl. Akad. Nauk SSSR* **215,** 366 (1974); UDC 541.183 (in English).
32. Block, J. H., Ehsasi, M., and Gorodetskii, V. V., *Prog. Surf. Sci.* **42,** 143 (1993).
33. Van Tol, M. F. H., Gielbert, A., and Nieuwenhuys, B. E., *Catal. Lett.* **16,** 297 (1992).
34. Van Tol, M. F. H., and Nieuwenhuys, B. E., *Appl. Surf. Sci.* **67,** 188 (1993).
35. Ehsasi, M., Berdau, M., Rebitzki, T., Charlé, K.-P., Christmann, K., and Block, J. H., *J. Chem. Phys.* **98,** 9177 (1993).
36. Eiswirth, M., Ph.D. thesis, Ludwig-Maximilians-Universität Munich (1987).
37. Ladas, S., Imbihl R., and Ertl, G., *Surf. Sci.* **198,** 42 (1988).
38. Van Tol, M. F. H., Siera, J., Cobden, P. D., and Nieuwenhuys, B. E., *Surf. Sci.* **274,** 63 (1992).
39. Gorodetskii, V., Drachsel, W., and Block, J. H., *Appl. Surf. Sci.* **76/77,** 122 (1994).
40. Nettesheim, S., von Oertzen, A., Rotermund, H. H., and Ertl, G., *J. Chem. Phys.* **98,** 9977 (1993).
41. Jakubith, S., Ph.D. thesis, FU Berlin (1991).
42. Ehsasi, M. Karpowicz, A., Berdau, M., Engel, W., Christmann, K., and Block, J. H., *Ultramicroscopy* **49,** 318 (1993).
43. Keil, W., and Wicke, E., *Ber. Bunsenges. Phys. Chem.* **84,** 377 (1980).